

UC Irvine

UC Irvine Previously Published Works

Title

GaSI: A Wide-Gap Non-centrosymmetric Helical Crystal.

Permalink

<https://escholarship.org/uc/item/6tk7j0zf>

Journal

Journal of the American Chemical Society, 146(33)

Authors

Dold, Kaitlyn

Cordova, Dmitri

Singsen, Sirisak

et al.

Publication Date

2024-08-21

DOI

10.1021/jacs.4c06487

Peer reviewed


GaSI: A Wide-Gap Non-centrosymmetric Helical Crystal


Kaitlyn G. Dold,[#] Dmitri Leo Mesoza Cordova,[#] Sirisak Singesen, Joseph Q. Nguyen, Griffin M. Milligan, Marcus Marracci, Ze-Fan Yao, Joseph W. Ziller, Dmitry A. Fishman, Elizabeth M. Y. Lee, and Maxx Q. Arguilla*


 Cite This: *J. Am. Chem. Soc.* 2024, 146, 22881–22886

 Read Online

ACCESS |

 Metrics & More

 Article Recommendations

 Supporting Information

ABSTRACT: The complex non-centrosymmetric and chiral nature of helical structures endow materials that possess such motifs with unusual properties. However, despite their ubiquity in biological and organic systems, there is a severe lack of inorganic crystals that display helicity in extended lattices, where these unusual properties are expected to be most pronounced. Here, we report a new inorganic helical structure, gallium sulfur iodide (GaSI), within the exfoliable class of III–VI–VII (1:1:1) one-dimensional (1D) van der Waals (vdW) crystals. Through detailed structural analyses, including single-crystal X-ray diffraction, electron microscopy, and density functional theory (DFT), we elucidate the apparent noncrystallographic screw axis and the first example of an atomic scale helical structure bearing a “*squirircular*” cross-section in GaSI. Crystallizing in the non-centrosymmetric $P\bar{4}$ space group, we found that GaSI crystals exhibit pronounced second-harmonic generation. From diffuse reflectance spectroscopy, GaSI displays a sizeable bandgap of 3.69 eV, owing to strong covalent interactions arising from the smaller sulfur atoms within the helix core. These results position GaSI as a promising exfoliable nonlinear optical material across a broad optical window.

Helical motifs, while often observed in biological or engineered molecules, remain elusive in dense inorganic crystals. Beyond their structural rarity, materials manifesting helical motifs have become sought after for the intrinsic lack of an inversion center, chiral/nonlinear vibrational and optical modes, topologically protected states, and potential for chiral-induced spin selectivity (CISS) behavior.^{1–14} Such properties are expected to be most pronounced in freestanding, all-inorganic lattices with atomic scale helicity. Helical hybrid organic–inorganic solids, including metal–organic frameworks, lack the exfoliability intrinsic to 1D vdW solids that enables long-range order at sub-nanometer structures and top-down access to enantiopure analogues.^{15,16} While hybrid coordination polymers are exfoliable, they are generally thermally unstable, lack delocalized states and long-range order, and are often not mechanically robust compared to helical 1D vdW crystals.^{17,18} More importantly, heavier elements in helical 1D vdW crystals impart stronger spin–orbit coupling to the system, which could enhance spin selectivity and chiral-induced properties.^{19–21} Nevertheless, building blocks of dense inorganic crystals lack the cooperative helicity-inducing interactions present in biological, organic, and hybrid supramolecular structures such as H-bonding and π – π stacking. As such, dense inorganic extended lattices with atomic scale helical motifs in weakly bound (noncovalent/ionic) chains are limited to elemental selenium, tellurium, and the rare double helix Sn(I/Br)P phase.^{7,8,22–26}

The case of the Sn(Br/I)P crystals suggests that the propagation of crystallographic screw axes along the long-axis of weakly bound chains leads to helical structures.^{8,22,23,27} Encouragingly, the immense interest in exfoliable 1D crystals has sparked the search for classes of inorganic crystals with sub-nanometer-thick chains held by vdW interactions.^{28–41}

Thus, the identification of screw axis symmetry within emergent 1D vdW crystal classes led to our discovery of helical motifs in III–VI–VII 1D vdW crystals (III = Al, Ga, In; VI = S, Se, Te; VII = Cl, Br, I).^{20,21,32,33,42–45} We found that crystals in this class manifest tetrahelical motifs along chains held by vdW interactions.^{20,21,32,42–45} For example, InSeI is a semiconductor consisting of periodic helical chains defined by a 4_1 screw axis and shows highly temperature-sensitive bandgaps in the visible range (Figure S1).^{20,21,32,42–44} Substitution of Ga atoms to the In site led to GaSeI, which is the first freestanding inorganic tetrahelix that is an approximate Boerdijk–Coxeter (B–C) helix.³³ B–C helices are characterized by a tetrahelix with vertices formed from a linear stack of ideal face-sharing tetrahedra with an angular displacement (or twist angle, θ_t) between two adjacent vertices defined by an irrational angle $\theta_t = \cos^{-1}(-2/3) \sim 131.81^\circ$, rendering the helix quasi-periodic. With this modularity, we leverage the critical role of the chalcogen atom (group VI) in directing the helicity of III–VI–VII crystals, expecting its profound influence on the helicity and crystal packing to be due to its role as one of the elements constituting the covalent chain scaffold.

Here, we describe the discovery and comprehensive characterization of GaSI, a wide-bandgap 1D vdW III–VI–VII crystal that displays a rare and unnatural helical motif

Received: May 14, 2024

Revised: July 15, 2024

Accepted: July 17, 2024

Published: July 22, 2024



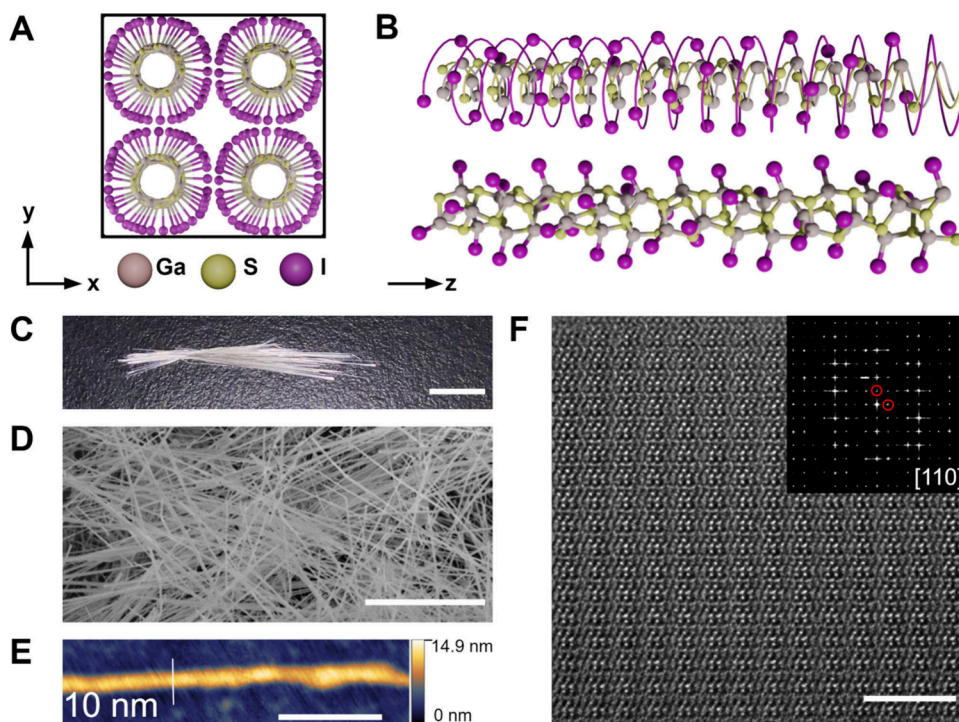


Figure 1. Crystal structure of the helical GaSI phase with the squirircular motif projected along the basal plane (A) and long-axis (B) directions. (C) GaSI bulk crystals grown from the melt. Scale bar, 5 mm. (D) SEM image of micromechanically unbundled GaSI nanowires. Scale bar, 50 μm (E) AFM image of ~ 10 nm-thick exfoliated GaSI nanowire. Scale bar, 500 nm. (F) HRTEM image of micromechanically exfoliated GaSI. Inset is the FFT with indexed (003) and (-110) periodic spots in red. Scale bar, 5 nm.

(Figure 1A,B). Through single crystal X-ray diffraction (SC-XRD), high-resolution transmission electron microscopy (HRTEM), second-harmonic generation (SHG) imaging, and density functional theory (DFT), we establish the structural helicity and the unusual “squirircular” helix cross-section in this unprecedented structure. We systematically elucidated the compositional dependence of the helicity and photophysical and nonlinear optical properties of GaSI compared to other III–VI–VII 1D vdW crystals.

Single crystals of GaSI were grown via a 500 $^{\circ}\text{C}$ melt of the constituent elements in a 1:1:1 ratio (Figure 1C). Colorless, fiber-like crystals retained their 1D morphology after micro-mechanical exfoliation, as evidenced by well-defined nanowires observed using scanning electron microscopy (SEM) (Figure 1D). These are exfoliable into nanowires with a thickness of ~ 10 nm through a sonication-assisted liquid-phase route (Figure 1E). Energy dispersive X-ray spectroscopy (EDS) and mapping, as well as X-ray photoelectron spectroscopy (XPS), confirm the elemental identity, oxidation states, 1:1:1 stoichiometric ratio, and uniform distribution of each element throughout analyzed crystals (Figures S2 and S3). HRTEM images of exfoliated GaSI crystals oriented along the [110] zone axis show that the crystalline order is retained upon exfoliation, with the covalent c -axis making up the long axis, implying its expected exfoliation along the a - and b -axes. HRTEM imaging also highlights the atomic-scale helical motif within the structure (Figure 1F). Persistent sharp peaks in the air exposure-dependent Raman spectra demonstrate the relative stability of GaSI crystals compared to GaSeI (Figure S4).³³

The refined unit cell of GaSI is characterized by two left-handed and two right-handed helices propagating along the z -axis which crystallize in the non-centrosymmetric tetragonal

space group, $P\bar{4}$ (No. 81; Figure 1A,B; Figure S5; Tables S2–S5). Each helix is constructed from corner-sharing GaS_3I quasi-tetrahedral building blocks with bridging sulfur atoms. Within each are three projectable concentric atomic tetrahelices comprising Ga, S, and I atoms that possess a unique set of helical parameters (radius, rise, and twist angle; Figure S6; Table S6). Ga and S atoms compose the inner cylinder of the helix, while the I atoms form the outer cylinder and are almost perpendicular to the long axis. The asymmetric unit is a helical tubule that displays noncrystallographic screw axes ($\sim 41_5$), with a $132(2)\dots^{\circ}$ twist angle between two consecutive Ga atoms within a helix. Adjacent chiral chains of opposing handedness are arranged in a primitive-like manner within an overall achiral but non-centrosymmetric unit cell.

The presence of bridging sulfur atoms in the helical chains composed of corner-sharing GaS_3I quasi-tetrahedral building units results in the unusual twisting of these units, opening of bridging Ga–S–Ga angles between units, and overall reconfiguration of the cross-sections of the constituent helices. We comprehensively compared the GaSI structure to the GaSeI B–C helix structure to systematically understand this distortion (Figure 2A–C). Based on the smaller atomic radius of S compared to Se, the constituent Ga, S, and I atomic tetrahelices in GaSI were expected to have smaller radii, given that there are no drastic changes in the structure of the asymmetric unit that were observable. Interestingly, only the radius of the chalcogen (S) atomic tetrahelix was reduced by 0.15 \AA (Figure 2B; Table S6), while the longest cross-sectional distance of the distorted Ga and I atomic tetrahelices remained generally unchanged. However, their cross-sectional motifs unexpectedly distorted into a Fernández-Guasti “squiracle” (Figure 2A,C, Table S6).⁴⁶

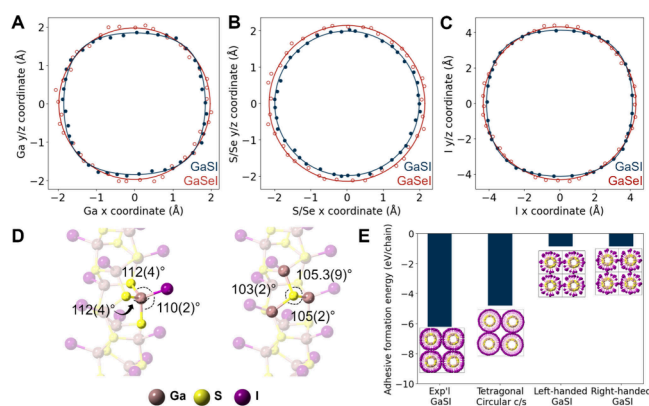


Figure 2. Cross-sections of the tetrahelices corresponding to the concentric Ga (A), chalcogen (S or Se; B), and I (C) elements in the GaSI (blue) and GaSeI (red) crystal structures. Filled (GaSI) and empty (GaSeI) circles correspond to experimental crystallographic positions, while lines correspond to fitted cross-sections. (D) Average experimental bond angles around the $[\text{GaS}_3\text{I}]_n$ and $[\text{Ga}_3\text{S}]_n$ polyhedral building units. (E) Calculated adhesive formation energies of the experimental GaSI structure bearing the squircular motif compared to several hypothetical structural models and packing motifs.

The squircle is a cross between a circle and a square mathematically described by eq 1:

$$r^2 = x^2 + y^2 - \frac{s^2}{r^2} x^2 y^2 \quad (1)$$

where r is the shortest path from the center to the edge of the squircle and s is the squareness factor. In this expression, $s = 1$ corresponds to a square and $s = 0$ to a circle. Fitting the cross-section of the GaSI helices results in a squareness factor of 0.69 and 0.65 for Ga and I cross-sections, respectively, which lies appreciably between a perfect square and a circle. The manifestation of a squircular helical motif in GaSI is the first of its kind and has never been observed at the atomic scale in

either naturally occurring or engineered helical crystals. The noncrystallographic nature of the screw axis (approximated as $\sim 41_{15}$), coupled with the twist angle and helical distortion, also suggests that GaSI exhibits a distorted B–C helix structure. We found through bond angle analysis in GaSI that the $[\text{GaS}_3\text{I}]_n$ quasi-tetrahedra remained rigid, while the $[\text{Ga}_3\text{S}]_n$ polyhedral subunits expanded, implying that the strain induced by the smaller S atoms (compared to Se) is accounted for by the increase in the Ga–S–Ga angles (Figure 2D; Table S7). This is enabled by the characteristic lattice flexibility between corner-sharing tetrahedra that possess tethering points (sulfur) that can be reconfigured to stabilize the rigid tetrahedral unit ($[\text{GaS}_3\text{I}]_n$).

To elucidate the origin of the unusual squircular distortion, we calculated from first-principles the adhesive formation energies of the experimental GaSI structure bearing the squircular cross-sectional motif and compared it with various hypothetical helical cross-sections and packing motifs using the following equation (eq 2):

$$E_{ad} = \frac{E_{bulk}(\text{GaSI}) - nE_{single-chain}(\text{GaSI})}{n} \quad (2)$$

where $E_{bulk}(\text{GaSI})$ is the energy of the bulk GaSI ($n = 4$ single chains of GaSI per unit cell) and $E_{single-chain}(\text{GaSI})$ is the energy of an individual one-dimensional chain. We found that the squircular helices packed with alternating handedness in the experimental tetragonal unit cell had the most negative adhesive formation energy (energetically favorable structure) compared to other hypothetical structures (Figure 2E; Figures S7 and S8; Supplementary Text A).

We also evaluated the role of vdW interactions in the stability of the squircular cross-sectional motif by computationally relaxing a single tetrahelix of GaSI in a vacuum and found that it relaxed to a helix with a circular and isotropic cross-section (Figure S9). This is indicative that weak interchain vdW interactions stabilize the squircular distortion within the cross-section of GaSI helices and suggests that the distortion arises to counteract the repulsive interactions within

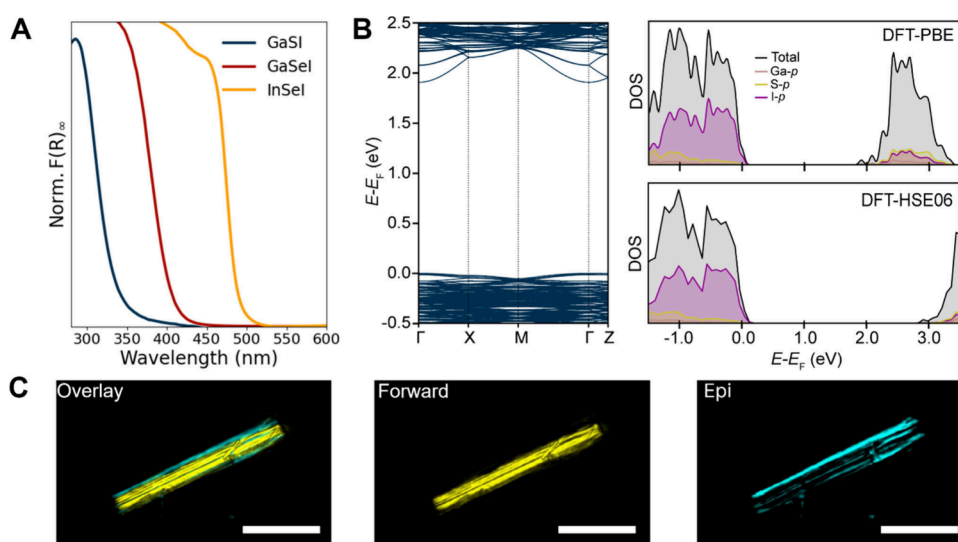


Figure 3. (A) DRS spectra of GaSI, GaSeI, and InSeI plotted in terms of the Kubelka–Munk function, $F(R)_\infty$. (B) DFT band structure and corresponding partial densities of states of GaSI, calculated with the PBE (top) functional and the HSE06 (bottom) functional. (C) Composite SHG micrograph of the forward (yellow) and epi (blue) channels taken at 400 nm from a micromechanically exfoliated GaSI microcrystallite. The forward (yellow) and epi (blue) channels are shown on the right. Scale bars: 40 μm .

the inner tubule of the chain (covalently bound Ga and S) and the angular strain introduced by the smaller bridging sulfur atom. We posit that the squircular distortion is facilitated by the highly reconfigurable corner-sharing tetrahedral motif, further stabilized by adjacent vdW interactions between oppositely handed chains. This unique structural motif presents several implications on the properties in the helix, as discussed in the Supporting Information (Figure S10; Supplementary Text B).

We also probed the photophysical properties of GaSI. Diffuse reflectance spectroscopy (DRS) of GaSI powders shows a significant and systematic widening of the bandgap with smaller group III and group VI atoms in the III–VI–VII class, from 2.45 eV in InSeI to 2.85 eV in GaSeI and, finally, 3.69 eV in GaSI (Figure 3A). To understand the origin of the wide bandgap of GaSI, we calculated the band structure and partial densities of states of GaSI, at first, using the generalized gradient approximation (Figure 3B). We found that GaSI is a direct bandgap semiconductor with a 1.9 eV bandgap, which, as expected, is underestimated using DFT at the generalized gradient approximation level, compared to DRS measurements. To this end, we performed hybrid DFT calculations, which show a similar orbital character from the densities of states plot (Figure 3B, right panel) but predict a sizable bandgap of 2.9 eV, which is comparable to experimental results. The wide bandgap develops from the stronger orbital overlap along the covalent direction arising from the smaller sulfur atom (Figure S1; Table S7).

Beyond potential applications in chiral-induced phenomena, the non-centrosymmetric packing from the helical chains in wide-bandgap GaSI makes it a suitable nonlinear optical (NLO) material that approaches the sub-nanoscale. These materials are of interest toward applications across a wide optical window including UV. The inherent non-centrosymmetric lattice of GaSI is poised to exhibit a nonzero second-order optical susceptibility and, hence, become optically active in NLO processes like second-harmonic generation. We confirm this assumption using SHG microscopy in both forward and epi detection modes, using an 800 nm femtosecond pulse as the fundamental excitation source (Figure 3C, Figure S11). GaSI crystals demonstrated a robust SHG response across a vast portion of micromechanically cleaved specimens. These experimental findings unequivocally validate the absence of inversion symmetry within the GaSI crystal structure (Figure S12). Low-dimensional solids exhibiting NLO properties remain a rarity, and materials that approach the theoretical limit have remained *in silico*.^{47,48} To our knowledge, GaSI is one of the first exfoliable 1D vdW solids to have experimental evidence for SHG and, in contrast to GaSeI, is significantly more air stable (Figure S4). We discuss the prospects of accessing enantiopure analogues of III–VI–VII 1D vdW helices in the Supporting Information (Figure S9; Supplementary Text C).

Altogether, we presented the creation of GaSI: a wide-bandgap, non-centrosymmetric, and exfoliable 1D vdW crystal with a unique “squircular” helical motif. This work demonstrates the realization of unusual helical motifs in dense inorganic solids and underscores the significant influence of constituent atoms on the crystal packing, helicity, and interchain interactions. Thus, the modularity of the tetrahedral building unit in III–VI–VII 1D vdW helices presents a chemical phase space to explore helical structures in inorganic

extended lattices, their ensuing properties, and applications in nonlinear optics and optoelectronic devices.

■ ASSOCIATED CONTENT

Supporting Information

The Supporting Information is available free of charge at <https://pubs.acs.org/doi/10.1021/jacs.4c06487>.

Geometry optimization and simulated thermal stability of GaSI crystals; implications of the squircular helical structure on properties; potential routes to access chiral forms of III–VI–VII 1D vdW helices; materials and methods; additional characterization and data: figures of crystal structures of helical 1D vdW lattices, InSeI, and GaSeI; EDS of GaSI crystals; XPS spectra of GaSI; air exposure-dependent Raman studies of GaSI crystals; thermal ellipsoid plot of the asymmetric unit derived from the single-crystal XRD refinement of GaSI; schematic of the helical parameters that define crystalline structures with tetrahedral geometries; minimum energy structure of GaSI from DFT calculations; time-dependent thermal stability of GaSI at 300 K; potential forms of chiral GaSI; calculated curvature and torsion of GaSI and GaSeI; schematic representation of the SHG microscopy setup used in the characterization of GaSI crystals in the Materials and Methods section; representative SHG micrographs of GaSI crystals obtained from the setup in Figure S4; tables of a summary of XPS peak parameters fitted using CasaXPS software; crystal data and structure refinement for mqa_GaSI_ACA; atomic coordinates and equivalent isotropic displacement parameters for mqa_GaSI_ACA; bond lengths and angles for mqa_GaSI_ACA; anisotropic displacement parameters for mqa_GaSI_ACA; fitted helix parameters, radii, and squareness factors of GaSI and GaSeI based on their parametric equations; average bond lengths and angles for the III–VI–VII compounds (PDF)

Accession Codes

CCDC 2354451 contains the supplementary crystallographic data for this paper. These data can be obtained free of charge via www.ccdc.cam.ac.uk/data_request/cif, or by emailing data_request@ccdc.cam.ac.uk, or by contacting The Cambridge Crystallographic Data Centre, 12 Union Road, Cambridge CB2 1EZ, UK; fax: +44 1223 336033.

■ AUTHOR INFORMATION

Corresponding Author

Maxx Q. Arguilla – Department of Chemistry, University of California, Irvine, California 92697, United States; Department of Chemical and Biomolecular Engineering, University of California, Irvine, California 92697, United States; orcid.org/0000-0001-9948-0814; Email: marguilla@uci.edu

Authors

Kaitlyn G. Dold – Department of Chemistry, University of California, Irvine, California 92697, United States
Dmitri Leo Mesoza Cordova – Department of Chemistry, University of California, Irvine, California 92697, United States; orcid.org/0000-0002-7527-8950

- Sirisak Singesen – Department of Materials Science and Engineering, University of California, Irvine, California 92697, United States
- Joseph Q. Nguyen – Department of Chemistry, University of California, Irvine, California 92697, United States; orcid.org/0000-0001-8058-7099
- Griffin M. Milligan – Department of Chemistry, University of California, Irvine, California 92697, United States; orcid.org/0000-0002-6632-8004
- Marcus Marracci – Department of Chemistry, University of California, Irvine, California 92697, United States
- Ze-Fan Yao – Department of Chemical and Biomolecular Engineering, University of California, Irvine, California 92697, United States; orcid.org/0000-0001-5590-0768
- Joseph W. Ziller – Department of Chemistry, University of California, Irvine, California 92697, United States; orcid.org/0000-0001-7404-950X
- Dmitry A. Fishman – Department of Chemistry, University of California, Irvine, California 92697, United States; orcid.org/0000-0001-6287-2128
- Elizabeth M. Y. Lee – Department of Materials Science and Engineering and Department of Chemical and Biomolecular Engineering, University of California, Irvine, California 92697, United States; orcid.org/0000-0001-9143-3140

Complete contact information is available at:
<https://pubs.acs.org/10.1021/jacs.4c06487>

Author Contributions

[#]K.G.D. and D.L.M.C contributed equally to this work.

Notes

The authors declare no competing financial interest.

ACKNOWLEDGMENTS

This work was supported by the National Science Foundation Materials Research Science and Engineering Center program through the UC Irvine Center for Complex and Active Materials under the award number DMR-2011967. G.M.M. is supported by the National Science Foundation Graduate Research Fellowship Program (2023331840). S.S. and E.M.Y.L. utilized the infrastructure for high-performance and high-throughput computing, research data storage and analysis, and scientific software tool integration built, operated, and updated by the Research Cyberinfrastructure Center (RCIC) at the University of California, Irvine (UCI). The RCIC provides cluster-based systems, application software, and scalable storage to directly support the UCI research community, <https://rcic.uci.edu>. We acknowledge the organizers of the 2023 ACA Summer Course in Chemical Crystallography held at Northwestern University, the Integrated Molecular Structure Education and Research Center (IMSERC) at Northwestern University, and its staff for generously lending their expertise in elucidating the structure presented in this work. J.Q.N. also acknowledges the UCI Chemistry Department's X-ray Crystallography Facility Fellowship for funding support. D.A.F. acknowledges the Chan-Zuckerberg Initiative grant 2023-321174 (5022) GB-1585590 for SHG imaging experiments. We also acknowledge the UC Irvine Department of Chemistry Laser Spectroscopy Laboratories for instrumental support. Several aspects of this work were performed at the UC Irvine Materials Research Institute (IMRI). Facilities and instrumentation at IMRI are supported, in part, by the National Science Foundation through the UC

Irvine Materials Research Science and Engineering Center grant number DMR-2011967. SEM-EDS was performed using instrumentation funded, in part, by the Chan-Zuckerberg Initiative grant 2023-321174 (5022) GB-1585590. XPS was performed using instrumentation funded in part by the National Science Foundation Major Research Instrumentation Program award number CHE-1338173.

REFERENCES

- (1) Tokura, Y.; Nagaosa, N. Nonreciprocal responses from non-centrosymmetric quantum materials. *Nat. Commun.* **2018**, *9* (1), 3740.
- (2) Liu, Y. Z.; Xiao, J. W.; Koo, J.; Yan, B. H. Chirality-driven topological electronic structure of DNA-like materials. *Nat. Mater.* **2021**, *20* (5), 638–644.
- (3) Mokashi-Punekar, S.; Zhou, Y. C.; Brooks, S. C.; Rosi, N. L. Construction of Chiral, Helical Nanoparticle Superstructures: Progress and Prospects. *Adv. Mater.* **2020**, *32* (41), No. 1905975.
- (4) Kuzyk, A.; Schreiber, R.; Fan, Z. Y.; Pardatscher, G.; Roller, E. M.; Hoge, A.; Simmel, F. C.; Govorov, A. O.; Liedl, T. DNA-based self-assembly of chiral plasmonic nanostructures with tailored optical response. *Nature* **2012**, *483* (7389), 311–314.
- (5) Chang, G. Q.; Wieder, B. J.; Schindler, F.; Sanchez, D. S.; Belopolski, I.; Huang, S. M.; Singh, B.; Wu, D.; Chang, T. R.; Neupert, T.; et al. Topological quantum properties of chiral crystals. *Nat. Mater.* **2018**, *17* (11), 978–985.
- (6) Naaman, R.; Waldeck, D. H. Chiral-induced spin selectivity effect. *Journal of physical chemistry letters* **2012**, *3* (16), 2178–2187.
- (7) Purschke, D. N.; Pielmeier, M. R.; Üzer, E.; Ott, C.; Jensen, C.; Degg, A.; Vogel, A.; Amer, N.; Nilges, T.; Hegmann, F. A. Ultrafast Photoconductivity and Terahertz Vibrational Dynamics in Double-Helix SnIP Nanowires. *Adv. Mater.* **2021**, *33* (34), No. 2100978.
- (8) Peng, B.; Murakami, S.; Monserrat, B.; Zhang, T. T. Degenerate topological line surface phonons in quasi-1D double helix crystal SnIP. *Npj Comput. Mater.* **2021**, *7* (1), 195.
- (9) Sutter, P.; Wimer, S.; Sutter, E. Chiral twisted van der Waals nanowires. *Nature* **2019**, *570* (7761), 354–357.
- (10) Liu, Y.; Wang, J.; Kim, S.; Sun, H. Y.; Yang, F. Y.; Fang, Z. X.; Tamura, N.; Zhang, R. P.; Song, X. H.; Wen, J. G.; et al. Helical van der Waals crystals with discretized Eshelby twist. *Nature* **2019**, *570* (7761), 358–362.
- (11) Göhler, B.; Hamelbeck, V.; Markus, T. Z.; Kettner, M.; Hanne, G. F.; Vager, Z.; Naaman, R.; Zacharias, H. Spin Selectivity in Electron Transmission Through Self-Assembled Monolayers of Double-Stranded DNA. *Science* **2011**, *331* (6019), 894–897.
- (12) Akopov, G.; Hewage, N. W.; Yox, P.; Viswanathan, G.; Lee, S. J.; Hulsebosch, L. P.; Cady, S. D.; Paterson, A. L.; Perras, F. A.; Xu, W.; et al. Synthesis-enabled exploration of chiral and polar multivalent quaternary sulfides. *Chem. Sci.* **2021**, *12* (44), 14718–14730.
- (13) Naaman, R.; Waldeck, D. H. Spintronics and Chirality: Spin Selectivity in Electron Transport Through Chiral Molecules. *Annu. Rev. Phys. Chem.* **2015**, *66*, 263–281.
- (14) Zhao, Y.; Zhang, C.; Kohler, D. D.; Scheeler, J. M.; Wright, J. C.; Voyles, P. M.; Jin, S. Supertwisted spirals of layered materials enabled by growth on non-Euclidean surfaces. *Science* **2020**, *370* (6515), 442–445.
- (15) Dong, L.; Chu, W.; Zhu, Q.; Huang, R. Three Novel Homochiral Helical Metal–Organic Frameworks Based on Amino Acid Ligand: Syntheses, Crystal Structures, and Properties. *Cryst. Growth Des.* **2011**, *11* (1), 93–99.
- (16) Zang, S.; Su, Y.; Li, Y.; Ni, Z.; Zhu, H.; Meng, Q. Interweaving of Triple-Helical and Extended Metal–O–Metal Single-Helical Chains with the Same Helix Axis in a 3D Metal–Organic Framework. *Inorg. Chem.* **2006**, *45* (10), 3855–3857.
- (17) Han, L.; Hong, M. Recent advances in the design and construction of helical coordination polymers. *Inorg. Chem. Commun.* **2005**, *8* (4), 406–419.

- (18) Wu, J.; Wang, N.; Xie, Y.-R.; Liu, H.; Huang, X.; Cong, X.; Chen, H.-Y.; Ma, J.; Liu, F.; Zhao, H.; et al. Polymer-like Inorganic Double Helical van der Waals Semiconductor. *Nano Lett.* **2022**, *22* (22), 9054–9061.
- (19) Hu, J.; Zhao, S.; Li, W.; Wang, H. Electronic states in one-dimensional helical crystals: General properties and application to InSeI. *Phys. Rev. B* **2024**, *109* (19), No. 195160.
- (20) Zhao, S.; Hu, J.; Zhu, Z.; Yao, X.; Li, W. Chirality-induced spin splitting in 1D InSeI. *Appl. Phys. Lett.* **2023**, *123* (17), No. 172404.
- (21) Zhou, Y.; Cordova, D. L. M.; Milligan, G. M.; Arguilla, M. Q.; Wu, R. Higher-dimensional spin selectivity in chiral crystals. *arXiv (Mesoscale and Nanoscale Physics)*. 2023-05–29. arXiv:2305.18637 (accessed 2024–06–24).
- (22) Pfister, D.; Schäfer, K.; Ott, C.; Gerke, B.; Pöttgen, R.; Janka, O.; Baumgartner, M.; Efimova, A.; Hohmann, A.; Schmidt, P.; et al. Inorganic double helices in semiconducting SnIP. *Adv. Mater.* **2016**, *28* (44), 9783–9791.
- (23) Reiter, F.; Pielmeier, M.; Vogel, A.; Jandl, C.; Plodinec, M.; Rohner, C.; Lunkenbein, T.; Nisi, K.; Holleitner, A.; Nilges, T. SnBrP-A SnIP-type representative in the Sn-Br-P system. *Z. Anorg. Allg. Chem.* **2022**, *648* (10), No. e202100347.
- (24) Ben-Moshe, A.; da Silva, A.; Muller, A.; Abu-Odeh, A.; Harrison, P.; Waelder, J.; Niroui, F.; Ophus, C.; Minor, A. M.; Asta, M.; et al. The chain of chirality transfer in tellurium nanocrystals. *Science* **2021**, *372* (6543), 729–733.
- (25) Ikemoto, H.; Fujimori, T.; Miyayama, T.; Kato, S.; Iesari, F.; Urita, K. Structures of Isolated Tellurium Chains Encapsulated Inside Carbon Nanotube. *J. Phys. Chem. C* **2020**, *124* (47), 26043–26047.
- (26) Churchill, H. O. H.; Salamo, G. J.; Yu, S. Q.; Hironaka, T.; Hu, X.; Stacy, J.; Shih, I. Toward Single Atom Chains with Exfoliated Tellurium. *Nanoscale Res. Lett.* **2017**, *12*, 488.
- (27) Müller, U. Die symmetrie von Spiralketten. *Acta Crystallogr. Sec. B* **2017**, *73* (3), 443–452.
- (28) Ghosh, S.; Kargar, F.; Sasing, N. R.; Barani, Z.; Salguero, T. T.; Yan, D.; Romyantsev, S.; Balandin, A. A. Low-Frequency Current Fluctuations in Quasi-1D (TaSe₃)₂ Weyl Semimetal Nanoribbons. *Advanced Electronic Materials* **2023**, *9* (2), No. 2200860.
- (29) Liu, G. X.; Romyantsev, S.; Bloodgood, M. A.; Salguero, T. T.; Shur, M.; Balandin, A. A. Low-Frequency Electronic Noise in Quasi-1D TaSe₃ van der Waals Nanowires. *Nano Lett.* **2017**, *17* (1), 377–383.
- (30) Balandin, A. A.; Kargar, F.; Salguero, T. T.; Lake, R. K. One-dimensional van der Waals quantum materials. *Mater. Today* **2022**, *55*, 74–91.
- (31) Cordova, D. L. M.; Chua, K.; Huynh, R. M.; Aoki, T.; Arguilla, M. Q. Anisotropy-Driven Crystallization of Dimensionally Resolved Quasi-1D Van der Waals Nanostructures. *J. Am. Chem. Soc.* **2023**, *145* (41), 22413–22424.
- (32) Cordova, D. L. M.; Zhou, Y.; Milligan, G. M.; Cheng, L.; Kerr, T.; Ziller, J.; Wu, R.; Arguilla, M. Q. Sensitive thermochromic behavior of InSeI, a highly anisotropic and tubular 1D van der Waals Crystal. *Adv. Mater.* **2024**, *36* (21), No. 2312597.
- (33) Cordova, D.; Chua, K.; Kerr, T.; Aoki, T.; Knez, D.; Skorupskii, G.; Lopez, D.; Ziller, J.; Fishman, D.; Arguilla, M. Atomically precise inorganic helices with a programmable irrational twist. *ChemRxiv (Materials Chemistry)*. 2024–02–22. 10.26434/chemrxiv-2024-n122g (accessed 2024–06–24).
- (34) Ogura, K. S.; Cordova, D. L. M.; Aoki, T.; Milligan, G. M.; Yao, Z.-F.; Arguilla, M. Q. Functionalization and Structural Evolution of Conducting Quasi-One-Dimensional Chevrel-Type Telluride Nanocrystals. *Chem. Mater.* **2024**, *36* (9), 4714–4725.
- (35) Allison, S. J.; Cordova, D. L. M.; Hasib, M.; Aoki, T.; Arguilla, M. Q. Nanoparticle-directed bimodal crystallization of the quasi-1D van der Waals phase, Bi₄I₄. *Chem. Sci.* **2024**, *15* (13), 4811–4823.
- (36) Milligan, G. M.; Yao, Z.-F.; Cordova, D. L. M.; Tong, B.; Arguilla, M. Q. Single Quasi-1D Chains of Sb₂Se₃ Encapsulated within Carbon Nanotubes. *Chem. Mater.* **2024**, *36* (2), 730–741.
- (37) Pham, T.; Reidy, K.; Thomsen, J. D.; Wang, B.; Deshmukh, N.; Filler, M. A.; Ross, F. M. Salt-assisted vapor-liquid-solid growth of one-dimensional van der Waals materials. *Adv. Mater.* **2024**, *36* (24), No. 2309360.
- (38) Island, J. O.; Molina-Mendoza, A. J.; Barawi, M.; Biele, R.; Flores, E.; Clamagirand, J. M.; Ares, J. R.; Sanchez, C.; van der Zant, H. S. J.; D'Agosta, R.; et al. Electronics and optoelectronics of quasi-1D layered transition metal trichalcogenides. *2D Mater.* **2017**, *4* (2), No. 022003.
- (39) Peng, B.; Xu, K.; Zhang, H.; Ning, Z. Y.; Shao, H. Z.; Ni, G.; Li, J.; Zhu, Y. Y.; Zhu, H. Y.; Soukoulis, C. M. 1D SbSeI, SbSI, and SbSBr With High Stability and Novel Properties for Microelectronic, Optoelectronic, and Thermoelectric Applications. *Adv. Theory Simul.* **2018**, *1* (1), No. 1700005.
- (40) Zhu, Y. B.; Rehn, D. A.; Antoniuk, E. R.; Cheon, G.; Freitas, R.; Krishnapriyan, A.; Reed, E. J. Spectrum of Exfoliable 1D van der Waals Molecular Wires and Their Electronic Properties. *ACS Nano* **2021**, *15* (6), 9851–9859.
- (41) Du, L. J.; Zhao, Y. C.; Wu, L. L.; Hu, X. R.; Yao, L. D.; Wang, Y. D.; Bai, X. Y.; Dai, Y. Y.; Qiao, J. S.; Uddin, M. G.; et al. Giant anisotropic photonics in the 1D van der Waals semiconductor fibrous red phosphorus. *Nat. Commun.* **2021**, *12* (1), 4822.
- (42) Sawitzki, G.; Muller, D.; Hahn, H. Crystal structures of InTeI and InSeI. *Mater. Res. Bull.* **1980**, *15* (6), 753–762.
- (43) Jiang, S.; Yin, H.; Zheng, G.-P.; Wang, B.; Guan, S.; Yao, B.-J. Computational prediction of a novel 1D InSeI nanochain with high stability and promising wide-bandgap properties. *Phys. Chem. Chem. Phys.* **2020**, *22* (46), 27441–27449.
- (44) Choi, K. H.; Cho, S.; Jeong, B. J.; Lee, B.; Jeon, J.; Kang, J.; Zhang, X.; Oh, H.-S.; Lee, J.-H.; Yu, H. K. One-dimensional van der Waals material InSeI with large band-gap for optoelectronic applications. *J. Alloys Compd.* **2022**, *927*, No. 166995.
- (45) Kniep, R.; Welzel, W. Phasenbeziehungen und intermediäre Verbindungen in Systemen GaX₃–Ga₂S₃ und InX₃–In₂S₃ (X= Cl, Br, I)/Phase Relations and Intermediate Compounds in Systems GaX₃–Ga₂S₃ and InX₃–In₂S₃ (X= Cl, Br, I). *Z. Naturforsch. B* **1985**, *40* (1), 26–31.
- (46) Fernández-Guasti, M. Analytic geometry of some rectilinear figures. *Int. J. Sci. Math. Educ.* **1992**, *23* (6), 895–913.
- (47) Liu, X.; Guo, Q.; Qiu, J. Emerging Low-Dimensional Materials for Nonlinear Optics and Ultrafast Photonics. *Adv. Mater.* **2017**, *29* (14), No. 1605886.
- (48) Yang, J.; Deng, J.; Pan, J.; Zhu, Y.; Zhang, Y.-F.; Li, Y.; Sun, J.-T.; Du, S. 1D Van der Waals Polymers with Nonlinear Optical Performance Approaching Theoretical Upper Limit. *Adv. Funct. Mater.* **2023**, *33* (48), No. 2305731.